Estimating longitudinal dispersion coefficients in natural channels

by

Yuqi Song

A thesis submitted to the graduate faculty

in partial fulfillment of the requirements for the degree of

MASTER OF SCIENCE

Major: Civil Engineering (Environmental Engineering)

Program of Study Committee:
Chris R. Rehmann, Major Professor
Roy Gu
Arka P. Ghosh

The student author, whose presentation of the scholarship herein was approved by the program of study committee, is solely responsible for the content of this thesis. The Graduate College will ensure this thesis is globally accessible and will not permit alterations after a degree is conferred.

Iowa State University

Ames, Iowa

2017

DEDICATION

This thesis is dedicated to my mother, Xiuling Feng, and my father, Lei Song. Thank you for supporting every of my decisions with trust and encouragement.

TABLE OF CONTENTS

LIST OF TABLES

LIST OF FIGURES

NOMENCLATURE

Roman symbols

$a_{0\text{-}4}$	estimated parameters in regression model
A	cross-sectional area of river channel
B	width of river channel
C	cross-sectional averaged concentration
C_{up}	unit peak concentration
D_y	transverse mixing coefficient
D_{y0}	parameter related to transverse mixing coefficient
DR	discrepancy ratio
E	matrix for errors of parameters estimation
f	friction factor
h	local flow depth
H	averaged channel depth
K	longitudinal dispersion coefficient
K_1	longitudinal dispersion coefficient for smooth channels (Wang & Huai 2016)
K_2	longitudinal dispersion coefficient for natural channels (Wang & Huai 2016)
K_{new1}	predicted longitudinal dispersion coefficient for smooth channels
K_{new2}	modified longitudinal dispersion coefficient for natural channels
K_p	longitudinal dispersion coefficient predicted from an empirical formula
K_m	longitudinal dispersion coefficient measured from experiments
K^*	integral part in dispersion equation
l	maximum distance from the bank to the peak velocity in the cross section

$r_{1,2}$	boundary layer control
R^2	coefficient of determination
S_0	longitudinal channel slope
S_f	bed shape factor
S_n	sinuosity
t	time
T_L	time of arrival the leading edge
T_P	time of arrival of the peak concentration
T_T	time of arrival of the trailing edge
T_{10}	time of arrival of a concentration equal to 10% of the peak
u	depth-averaged streamwise velocity
$\hat{u}$	dimensionless depth-averaged streamwise velocity
u'	deviation of the depth-averaged velocity from the cross-sectional average
$\hat{u}'$	dimensionless deviation of the depth-averaged velocity from the cross-sectional average
u_*	shear velocity
U	cross-sectional average velocity
x	coordinate in streamwise direction
x_i	explanatory variables
X_i	matrices of explanatory variables
y	coordinate in transverse direction
Y	matrix of estimators

Greek symbols

α	dimensionless coefficient related to transverse mixing
β_i	estimated parameters in regression model
δ	boundary layer thickness
ε	error of parameter estimation
ϕ_2	secondary flow coefficient
λ	dimensionless transverse eddy viscosity
η	dimensionless coordinate in transverse direction
μ	dynamic viscosity
μ_t	time of passage of the centroid
ρ	fluid density
σ_t^2	temporal variance of time
τ_0	bottom shear stress
τ_{yx}	depth-averaged transverse Reynolds stress
$\omega_d^{1/2}$	peak velocity of velocity profile
$\psi_{1,2}$	revision coefficients in Wang & Huai model (2016)

Other notation

ADCP	acoustic Doppler current profiler
ADV	advection-dispersion equation
AIC	Akaike's information criterion
SBC	Schwarz's Bayesian criterion
$\overline{u}\,\overline{v}$	product of averaged longitudinal and transverse velocities
$\overline{u}\,\overline{w}$	product of averaged longitudinal and vertical velocities
$\overline{u'v'}$	averaged product of fluctuations of longitudinal and transverse velocities
$\overline{u'w'}$	averaged product of fluctuations of longitudinal and vertical velocities
$\left(\overline{u}\cdot\overline{v}\right)_d$	depth-averaged velocity component

ACKNOWLEDGMENTS

I would like to thank Iowa State University (ISU) for providing such friendly, harmonious, and inclusive studying environment for me as an international student. The four and half years that I spent here would be one of the most memorable pages in my life. I remember every single footprint here at Iowa State, which are not just about failures and achievements but tears and joys. Especially, I want to acknowledge the Department of Civil, Construction and Environmental Engineering and the International Students and Scholars Office. They have always shown stances of being helpful and understanding, and made me feel much easier and relaxing as a foreign student.

My advisor, Dr. Chris Rehmann, played unique role in my journey of studying abroad since he enlightened me with his wisdom, humor, and endless patience. With his advice and help, I'm getting close to the kind of person I want to be, and I will continue improving myself to be a person like my advisor. I greatly thank him about things that he had done for me including asking funding for me from every place that he could think of, large amount of time input on revising my thesis and meeting with me during his busiest period, always being patient when I asked some silly questions, sometimes being my English teacher, etc.

I would like to thank Dr. Kenneth Koehler for his four-hour help in order to obtain the regression model. I also want to acknowledge other committee members, Dr. Gu and Dr. Ghosh; thanks go to them for being on my defense and sharing some valuable insights.

I also would like to thank my academic family—Cindy, Lauren and Rusen for giving feedback on thesis improvement, the warm support during my defense, and two years consistent help.

In addition, I want to thank Dr. Ikuma for sharing her academic experiences and providing helpful advice. Dr. Ong also gave me lots of advice when I started running the Water Environment Federation Student Chapter at ISU, and I had learned a lot from working with him. Dr. Alleman never hesitated to share his experiences and to make a sense of humor, and it was an enjoyable experience to have his classes.

There were a lot of people helping my master program moving smoothly, such as Kathy, Nancy and Emma. Kendra, Jess, April and Marva also helped me a lot when I met problems.

ABSTRACT

A new empirical formula is developed for estimating the longitudinal dispersion coefficient. Velocity profiles are computed from the momentum equation as presented by Shiono and Knight (1991), and the dispersion coefficient is computed from the velocity profiles using the theory of shear dispersion (Taylor 1953, Fischer et al. 1979). To simplify the application, results of the numerical integration are expressed in terms of the aspect ratio of the channel, the friction factor, the dimensionless eddy viscosity, and the secondary flow coefficient using multiple regression. For laboratory data, 83.3% of the empirical estimates from the initial formula fall within 50% of values from tracer measurements. After adjustment of the initial formula, the second formula predicts the data of Nordin and Sabol (1974) as well as the formula of Wang and Huai (2016). For example, both the proposed formula and the formula of Wang and Huai (2016) have mean and median values of the discrepancy ratio of −0.12 and standard deviation less than 0.5.

CHAPTER 1. INTRODUCTION

Motivation and Significance

The longitudinal dispersion coefficient is a key parameter for quantifying spreading of pollutants during transport in rivers and streams, and this research aims to improve the estimation of the longitudinal dispersion coefficient. The change of the concentration of a conservative pollutant in rivers and streams depends on advection by the flow and spreading by several mechanisms, including shear dispersion and interaction with recirculation zones. The advection-diffusion model, derived from conservation of contaminant mass, can provide an analytical solution for the pollutant concentration as a function of time and distance from the injection. Because the analytical solution involves the longitudinal dispersion coefficient as a parameter; estimating the longitudinal dispersion coefficient is critical for predicting the pollutant concentrations.

Several methods are used to determine the longitudinal dispersion coefficient: tracer studies, the acoustic Doppler current profiler (ADCP) method, the USGS/Jobson method, and empirical formulas. Tracer studies give the best estimates because they can measure the effect of recirculation zones and other factors leading to dispersion. The ADCP method usually underestimates the dispersion coefficient since it does not consider the effects of recirculation zones. Empirical formulas save time and labor, as well as costs compared to tracer studies and the ADCP method. Also, some empirical estimates are more accurate than the USGS/Jobson method. Still, the estimates from empirical formulas can be improved. For example, commonly used formulas estimate the dispersion coefficient with a mean absolute error of 37-320% (Wang and Huai 2016).

Most empirical formulas account for the properties of the flow and geometry of the channel, but they express the dispersion coefficient in terms of only the ratio of the mean velocity and shear velocity and the ratio of channel width and channel depth. The scatter in the predictions and the differences between predicted and measured values of the dispersion coefficient suggest that other parameters may be important. In fact, the momentum equation used by Wang and Huai (2016) accounted for transverse turbulent momentum flux (as quantified by the transverse eddy viscosity) and secondary flow, though their proposed formula for the dispersion coefficient did not. To improve accuracy of estimating the dispersion coefficient, a new formula is developed in this study considering secondary flow and eddy viscosity.

Objectives

This study will determine the effect of secondary flow and the dimensionless eddy viscosity on the dispersion coefficient. The research aims to develop a new formula for the dispersion coefficient that will provide better estimates than other empirical estimates.

Hypotheses

The hypothesis behind this work is that estimates of the longitudinal dispersion coefficient can be improved by including the effects of transverse turbulent momentum flux and secondary flow. The former is characterized by the dimensionless eddy viscosity, and the latter is characterized by the secondary flow coefficient. These parameters will be defined precisely in Chapters 2 and 3.

Outline of Thesis

The work will be presented in four parts. Chapter 2 will include background information, such as basic concepts about dispersion, methods for estimating the dispersion coefficient, and a discussion of empirical formulas. Methods to obtain a new formula will be explained in chapter 3. Results and discussion will be combined in chapter 4 to analyze results and to improve the performance of the initial formula. Conclusions are presented in Chapter 5.

CHAPTER 2. BACKGROUND

Mechanisms of Dispersion

Shear Dispersion

The interaction of transverse mixing with velocity gradients across a channel produces shear dispersion, a primary cause of longitudinal spreading of contaminants (Rutherford 1994, p. 179). Mixing in the transverse direction *y* causes a parcel of tracer to sample different velocities, and after enough time has passed, the tracer cloud will spread in the streamwise direction *x*. Thus, if transverse mixing (as measured by the transverse mixing coefficient D_y) is large, tracer parcels will sample more of the velocities, and shear dispersion will be diminished. In contrast, if the transverse mixing is small, differences in the velocities between tracer parcels will be larger, and shear dispersion will increase.

Taylor (1954) quantified shear dispersion in a pipe by analyzing the deviations of the velocity and concentration from their cross-sectional averages *U* and *C*. Beyond a certain distance, the longitudinal flux of contaminant can be expressed as proportional to the streamwise concentration gradient; the coefficient of proportionality is the longitudinal dispersion coefficient *K*. Fischer (1967) extended this concept to rivers and wrote the dispersion coefficient as

$$K = -\frac{1}{A}\int_0^B u'(y)h(y)\int_0^y \frac{1}{D_y h(y)}\int_0^y u'(y)h(y)dydydy \qquad (2.1)$$

where *y* is the transverse coordinate starting at the bank, *B* is the width of the channel, *A* is the cross-sectional area, $h(y)$ is the local flow depth, D_y is the transverse mixing coefficient, and $u'(y) = u(y) - U$ is the deviation of the depth-averaged velocity $u(y)$ from the cross-

sectional average. Expressing the flux in this way allows the concentration to be predicted from the one-dimensional advection-dispersion equation (ADE):

$$\frac{\partial C}{\partial t} + U\frac{\partial C}{\partial x} = K\frac{\partial^2 C}{\partial x^2} \tag{2.2}$$

where t is time. The ADE is widely used to predict the transport of pollutants despite the challenge of specifying the dispersion coefficient K.

Recirculation Zones

Recirculating flows happen near river bends and in side embayments and other irregularities in channels, and tracer is likely to be trapped in these regions, which are called recirculation zones (Rutherford 1994). Recirculation zones violate an assumption of Eq. (2.2), the homogeneity of turbulent flows. Although the recirculation zone is modeled as uniform along the channel (e.g., Rutherford 1994), they occur sporadically in natural channels. Additionally, the rate of exchange in and out of recirculation zones is small; therefore, once tracer is trapped in the recirculation zone, the releasing time is extended.

Estimates of Dispersion

Tracer Studies

Tracer studies are widely used to estimate the longitudinal dispersion coefficient. Many tracers have been used to measure spreading, but fluorescent dyes, such as Rhodamine WT, are most common because they can be measured at low concentration (Rutherford 1994, p. 235). The response curve of a tracer is obtained by measuring the concentration at certain downstream distances for a period of time. Then the dispersion coefficient can be determined with the method of moments or by routing (Rutherford 1994, ch. 4).

Tracer studies have several advantages and disadvantages. Tracer studies are considered more accurate than other methods because they account for the conditions for the specific reach of the river being investigated, including the geometry, flow, and weather (Carr and Rehmann 2007). However, for the same reason the results from tracer studies are restricted to those conditions. Tracer studies are relatively easy to conduct for small streams, and the tracer input rate can be optimized to account for the conditions in the field (Rutherford 1994). Rutherford (1994, ch. 5) outlined several challenges with tracer studies: (1) The planning, costs, labor, and coordination increase with the size of the river; (2) multiple tracer studies are needed under different conditions to obtain more general information about dispersion in the river; (3) a study must be designed to account for trapping of tracer in sediments or vegetated areas; and (4) in studies with natural tracers, the background concentrations in the main channel and tributaries must be determined.

Acoustic Doppler Current Profiler

The acoustic Doppler current profiler (ADCP) method serves as an alternative way to estimate the longitudinal dispersion coefficient *K*. Fischer et al. (1979, p. 130) described using velocities measured with propeller meters to compute *K* using the theory of shear dispersion. Exploiting the ability of an ADCP to provide velocity profiles with higher spatial resolution, Bogle (1997) used measurements from an ADCP to estimate *K* in the Sacramento Delta, and Carr and Rehmann (2007) and Shen et al. (2010) refined and evaluated the method thoroughly.

The ADCP uses the Doppler effect to measure three components of velocity. As an ADCP moves across a cross section of a river, it emits a sequence of high frequency sounds underwater; meanwhile moving particles in the river reflect the sound back to the ADCP with

a different frequency. The instrument detects and uses the Doppler shift to compute velocities in various depth bins so that a detailed velocity profile can be developed for the cross section of the river. The velocity profile is used along with an estimate of the transverse mixing coefficient in the theory of shear dispersion, as expressed in Eq. (2.1), to compute the longitudinal dispersion coefficient (e.g., Carr and Rehmann 2007).

On one hand, the ADCP serves as an excellent option instead of tracer studies since the ADCP can obtain a relatively accurate result by measuring and averaging the velocities of multiple transections. On the other hand, the ADCP cannot measure velocity profiles near the river bed and shallow stream reaches (Shen et al. 2010).

USGS/Jobson Method

Jobson (1996) documented a method used by the United States Geological Survey (USGS) to predict longitudinal dispersion from time-of-travel studies in rivers and streams. The tracer-response curve is represented as a scalene triangle by specifying the time of arrival the leading edge (T_L), the time of arrival of the peak concentration (T_P) and the unit-peak concentration C_{up}, and the time of arrival of the trailing edge, taken as the time of arrival (T_{10}) of a concentration equal to 10% of the peak. The concentration is zero before the leading edge and after the trailing edge. Using data compiled by Nordin and Sabol (1974), Jobson (1996) related the velocity of the peak concentration to parameters mostly available at gaging stations: drainage area, reach slope, mean annual river discharge, and the discharge at the time of the measurement. Once the time of the peak is known, then other parameters specifying the tracer response curve can be computed.

Predictions from the method of Jobson (1996) can be related to the parameters of the ADE by considering the temporal moments of the tracer response curve. The time of arrival

of the trailing edge T_T, where the concentration is zero, can be calculated by using similar triangles:

$$\frac{T_T - T_P}{T_{10} - T_P} = \frac{C_{up}}{0.9C_{up}} = 1.11 \tag{2.3}$$

The longitudinal dispersion coefficient K can be calculated from the time of passage of the centroid (μ_t) and the temporal variance σ_t^2, which for the triangle are given by

$$\mu_t = \frac{T_L + T_P + T_T}{3} \tag{2.4}$$

and

$$\sigma_t^{\,2} = \frac{1}{18}(T_L^{\,2} + T_P^{\,2} + T_T^{\,2} - T_L T_P - T_L T_T - T_T T_P) \tag{2.5}$$

Then, neglecting the initial variance and using the frozen cloud approximation gives

$$K = \frac{U^2 \sigma_t^{\,2}}{2\mu_t} \tag{2.6}$$

These equations connect the Jobson method to the ADE.

Empirical Formulas

Early attempts to develop formulas to predict the dispersion coefficient include the work of Elder (1959) and Fischer et al. (1979). Elder (1959) focused on the vertical variation of velocity and excluded the transverse variation to find

$$K = 5.93 H u_* \tag{2.7}$$

where H is averaged channel depth. However, because the transverse variation is more important for dispersion in rivers (Fischer et al. 1979; Rutherford 1994), Elder's formula is not usually used.

The formula of Fischer et al. (1979) is based on approximating Eq. (2.1) as

$$K = \frac{0.07\sqrt{\overline{u'^2}}\,l^2}{D_y}$$

where l is the maximum distance from the bank to the peak velocity in the cross section. Using the observed ranges $0.23 < D_y / u_* H < 0.7$ and $0.17 < \overline{u'^2} / U^2 < 0.25$, Fischer et al. (1979) chose $D_y = 0.6 u_* H$, $\overline{u'^2} / U^2 = 0.2$, and $l \approx 0.7B$ to obtain

$$\frac{K}{u_* H} = 0.011 \left(\frac{B}{H} \right)^2 \left(\frac{U}{u_*} \right)^2 \tag{2.8}$$

This formula has been used extensively. For example, the Incident Command Tool for Drinking Water Protection (Samuels et al. 2015) employs Eq. (2.8) to compute the evolution of a contaminant cloud after a spill.

Several researchers have used dimensional analysis and regression to develop formulas for the dispersion coefficient using the compilation of Nordin and Sabol (1974), which consists of 59 datasets measured from 26 U.S. rivers. Seo and Cheong (1998) related the dispersion coefficient to properties of the flow (U and u_*), properties of the fluid (density ρ and dynamic viscosity μ), and channel geometry (B, H, bed shape factor S_f, and sinuosity S_n). Dimensional analysis then yielded

$$\frac{K}{u_* H} = f_1 \left(\rho \frac{UH}{\mu}, \frac{U}{u_*}, \frac{B}{H}, S_f, S_n \right) \tag{2.9}$$

The bed shape factor and sinuosity describe irregularities in natural streams, especially those that can cause secondary flow. Seo and Cheong (1998) dropped S_f and S_n because they are not easy to obtain, and they also neglected the Reynolds number because it had a negligible effect on the longitudinal dispersion. Then Eq. (2.13) was simplified to

$$\frac{K}{u_* H} = f_2\left(\frac{U}{u_*}, \frac{B}{H}\right) \tag{2.10}$$

By applying robust estimation to Eq. (2.14) the dispersion coefficient was expressed as

$$\frac{K}{u_* H} = 5.915\left(\frac{B}{H}\right)^{0.620}\left(\frac{U}{u_*}\right)^{1.428} \tag{2.11}$$

Kashefipour and Falconer (2002) exploited the success of Eq. (2.11) in developing their own formula. Similar dimensional analysis and regression between *HU* and *BU* versus *K* produced

$$K = 10.612 HU(\frac{U}{u_*}) \tag{2.12}$$

To assess the performance of empirical formulas, Kashefipour and Falconer (2002), as well as others, used the discrepancy ratio (DR):

$$\mathrm{DR} = \log_{10}\left(\frac{K_p}{K_m}\right) \tag{2.13}$$

where K_p is the longitudinal dispersion coefficient predicted from an empirical formula and K_m is the longitudinal dispersion coefficient measured from experiments. Perfect agreement gives DR = 0, while underestimates give DR < 0 and overestimates give DR > 0. By conducting the discrepancy ratio test, Kashefipour and Falconer (2002) found Eq. (2.11) overestimated and Eq. (2.12) underestimated. Their proposed formula results from a linear combination of Eqs. (2.11) and (2.12):

$$\frac{K}{u_* H} = \left[7.428 + 1.775\left(\frac{B}{H}\right)^{0.620}\left(\frac{u_*}{U}\right)^{0.572}\right]\left(\frac{U}{u_*}\right)^2 \tag{2.14}$$

Some researchers have used the theory of shear dispersion to develop formulas for the dispersion coefficient. Deng et al. (2001) brought the shape factor into the analysis by

specifying a symmetric function to describe the shape of the channel. They also assumed a velocity profile based on applying Manning's equation locally in the cross section and developed a formula for the transverse mixing coefficient, given by $D_y = D_{y0} u_* h(y)$, where

$$D_{y0} = 0.145 + \frac{1}{3,520}\left(\frac{B}{H}\right)^{1.38}\frac{U}{u_*} \tag{2.15}$$

The result of using this information in Eq. (2.1) involved a complicated numerical integral, which Deng et al. (2001) expressed as a function of *B*/*H*. Their proposed formula is

$$\frac{K}{u_* H} = \frac{0.15}{8D_{y0}}\left(\frac{B}{H}\right)^{5/3}\left(\frac{U}{u_*}\right)^2 \tag{2.16}$$

The numerical coefficient 0.15 in Eq. (2.16) is the product of 0.01, which arises from the semi-theoretical analysis, and a "revision constant" of 15, which Deng et al. (2001) introduced to account for the difference between smooth and rough channels observed by Fischer (1967).

Rather than specify a velocity profile, Wang and Huai (2016) computed a velocity profile by solving the momentum equation of Shiono and Knight (1991). For steady uniform turbulent flow, the streamwise momentum equation is

$$\rho\left(\frac{\partial}{\partial y}\left(\overline{u}\,\overline{v}\right) + \frac{\partial}{\partial y}\left(\overline{u}\,\overline{w}\right)\right) = \rho g S_0 + \frac{\partial}{\partial y}\left(-\rho\overline{u'v'}\right) + \frac{\partial}{\partial z}\left(-\rho\overline{u'w'}\right) \tag{2.17}$$

where the overbar denotes a time average, primes denote fluctuations from the time average, ρ is water density, g is the acceleration of gravity, and S_0 is the longitudinal channel slope. Shiono and Knight (1991) integrated Eq. (2.17) over the depth to obtain

$$\rho g H S_0 - \tau_0 + \frac{\partial}{\partial y}\left(H\tau_{yx}\right) = \frac{\partial}{\partial y}\left[H\left(\rho\overline{u}\cdot\overline{v}\right)_d\right] \tag{2.18}$$

where τ_0 is the bottom shear stress, τ_{yx} is the depth-averaged transverse Reynolds stress, and the subscript d denotes a depth average. In obtaining this version of the momentum equation the sides of the channel are assumed to be vertical. In Eq. (2.18) the first term on the left is the component of the fluid's weight in the streamwise direction; the second term is the bed shear stress; the third term involves transverse momentum transport by Reynolds shear stress; and the term on the right is related to secondary flow, which can occur at bends in rivers because of pressure gradients that drive transverse flow. Following Shiono and Knight (1991), Wang and Huai (2016) expressed the bottom shear stress in terms of a friction factor *f*:

$$\tau_0 = \frac{f}{8}\rho U^2 \tag{2.19}$$

They introduced the shear velocity u_* as a measure of bottom shear stress:

$$u_* = \sqrt{\frac{\tau_0}{\rho}} \tag{2.20}$$

and computed the Reynolds shear stress with an eddy viscosity:

$$\tau_{yx} = \rho\lambda u_* H\frac{\partial u}{\partial y} = \rho\lambda\left(\frac{f}{8}\right)^{\frac{1}{2}} uH\frac{\partial u}{\partial y} \tag{2.21}$$

where λ is the dimensionless transverse eddy viscosity and u is the depth-averaged streamwise velocity. Inserting Eqs. (2.19) and (2.21) into Eq. (2.18) gives

$$\rho g H S_0 - \frac{1}{8}\rho f u^2 + \frac{\partial}{\partial y}\left[\rho\lambda H^2\left(\frac{f}{8}\right)^{1/2} u\frac{\partial u}{\partial y}\right] = \rho\frac{\partial}{\partial y}\left[H(\bar{u}\cdot\bar{v})_d\right] \tag{2.22}$$

Several researchers have used forms of Eq. (2.22) to study the transverse variation of velocity in channels (e.g., Shiono and Knight 1991, Ervine et al. 2000).

Wang and Huai (2016) determined the velocity profile for cases in which the secondary flow [i.e., the term on the right side of Eq. (2.22)] can be neglected. To facilitate the integration required by applying Eq. (2.1), they expressed the velocity profile in terms of Fourier series, and to simplify the calculation of the dispersion coefficient, they assumed that the integral depends only on *B/H*. As noted above, Deng et al. (2001) used a similar approach, though with a different velocity profile. These calculations yielded a formula for the dispersion coefficient K_1 in a rectangular flume, and Wang and Huai (2016) used regression analysis and the maximum-dissimilarity algorithm to determine the dispersion coefficient K_2 for natural channels. In particular, they used

$$\ln\left(\frac{K_2}{u_* H}\right) = \psi_1 \ln\left(\frac{K_1}{u_* H}\right) + \psi_2 \tag{2.23}$$

with $\psi_1 = 0.5815$ and $\psi_2 = 4.3223$ to obtain

$$\frac{K}{u_* H} = 17.648\left(\frac{B}{H}\right)^{0.3619}\left(\frac{U}{u_*}\right)^{1.16} \tag{2.24}$$

Wang and Huai (2016) used the mean error rate and mean absolute error rate with several datasets to show that Eq. (2.24) predicts the dispersion coefficient better than other formulas.

Summary

The previous models considered the variation of dispersion coefficient with *B/H* and U / u_*; however, none of the previous work analyzed eddy viscosity and secondary flow as variables in these models. Therefore, this study will explore a new equation for the dispersion coefficient that includes more parameters—specifically, those describing momentum transport by eddies and secondary flow—in order to improve the accuracy of empirical estimates.

CHAPTER 3. METHODS

This section explains the methods to obtain the new model for the dispersion coefficient. The streamwise momentum equation as presented in Eq. (2.22) is used to calculate the velocity profile, which is then used to compute the dispersion coefficient as a function of four main variables with the key result from the theory of shear dispersion, Eq. (2.1). A function describing the dependence of the dispersion coefficient on the four variables is determined with regression analysis.

Calculation of Velocity Profile

As in Wang and Huai (2016), the velocity profile is computed from a version of the momentum equation from Shiono and Knight (1991). To include the effects of secondary flow, the last term in Eq. (2.22) is expressed with the formulation of Ervine et al. (2000):

$$(\overline{u}\cdot\overline{v})_d = \phi_2 u^2 \tag{3.1}$$

where ϕ_2 is the secondary flow coefficient. Inserting Eq. (3.1) into Eq. (2.22) yields

$$\rho g H S_0 - \frac{1}{8}\rho f u^2 + \frac{\partial}{\partial y}\left[\rho\lambda H^2\left(\frac{f}{8}\right)^{1/2} u\frac{\partial u}{\partial y}\right] = \rho\frac{\partial}{\partial y}(H\phi_2 u^2) \tag{3.2}$$

This second order linear differential equation has been solved by several researchers (e.g., Shiono and Knight 1991, Ervine et al. 2000, Wang and Huai 2016); here the solution is written as

$$u = \omega_d^{1/2}\left(\frac{e^{r_2}-1}{e^{r_1}-e^{r_2}}e^{\frac{y}{B}r_1} + \frac{1-e^{r_1}}{e^{r_1}-e^{r_2}}e^{\frac{y}{B}r_2} + 1\right)^{1/2} \tag{3.3}$$

where $\omega_d = 8gHS_0/f$ and r_1 and r_2 are given by

$$r_{1,2} = \frac{1}{\lambda}\frac{B}{H}\left(\frac{8}{f}\right)^{\frac{1}{2}}\left(\phi_2 \pm \sqrt{\phi_2^2 + \frac{\lambda f}{4}\left(\frac{f}{8}\right)^{\frac{1}{2}}}\right) \tag{3.4}$$

The velocity profile is written in a dimensionless form by normalizing by $\sqrt{gHS_0}$. Then the dimensionless velocity $\hat{u}$ is

$$\hat{u} = \left(\frac{8}{f}\right)^{1/2}\left(\frac{e^{r_2}-1}{e^{r_1}-e^{r_2}}e^{r_1\eta} + \frac{1-e^{r_1}}{e^{r_1}-e^{r_2}}e^{r_2\eta} + 1\right)^{1/2} \tag{3.5}$$

where $\eta = y / B$ is a dimensionless transverse coordinate starting at a bank.

Calculation of Dispersion Coefficient

The dispersion coefficient is computed using the theory of shear dispersion, which results in Eq. (2.1). In this study, the channel is assumed to be rectangular. Therefore, the local depth does not change across the channel, and Eq. (2.1) can be written as

$$K = -\frac{1}{D_y B}\int_0^B u' \int_0^y \int_0^y u' dy dy dy \tag{3.6}$$

In dimensionless terms Eq. (3.6) can be expressed as

$$K^* = \frac{KD_y}{gHS_0B^2} = -\int_0^1 \hat{u}' \int_0^\eta \int_0^\eta \hat{u}' d\eta d\eta d\eta \tag{3.7}$$

where $\hat{u}'$ is the deviation of the dimensionless velocity from the cross-sectional average. The transverse mixing coefficient is taken to be proportional to the transverse eddy viscosity so that $D_y = \alpha\lambda u_* H$, in which α is a dimensionless coefficient. The product $\alpha\lambda$ denoted as D_{y0} in Eq. (2.15) is approximately 0.15 for straight channels and 0.6 for meandering rivers (Fischer et al. 1979; Shiono & Knight 1991). This formulation suggests that the dimensionless dispersion coefficient K^* is a function of four parameters:

$$K^* = F\left(\frac{B}{H}, \frac{U}{u_*}, \lambda, \phi_2\right) \tag{3.8}$$

That is, K^* depends on the aspect ratio of the channel, the friction factor (which is related to U / u_*), the dimensionless eddy viscosity, and the secondary flow coefficient. The function F was determined numerically by Matlab with the four parameters given as inputs, and the codes are attached in Appendix A.

Regression Method for K^*

Obtaining an analytical solution of K^* is difficult due to the triple integration in Eq. (3.7). Therefore, K^* is computed by numerical integration, and a multiple regression model is introduced to estimate K^* by using selected data. This section includes the processes for estimating the model (e.g., building the regression model), selecting the data, and comparing the regression models.

Multiple Regression Model

When a dependent variable y is a linear function of n explanatory variables x_1, x_2,…, x_n,

$$y = \beta_0 + \beta_1 x_1 + \beta_2 x_2 + \cdots + \beta_n x_n + \varepsilon \tag{3.9}$$

(where ε is the error from parameter estimation), then multiple regression can be used to estimate the unknown parameters β_0, β_1, β_2,…, β_n in Eq. (3.9). Once m observations occur, the multiple regression can be expressed in a matrix form:

$$Y = \beta_0 + \beta_1 X_1 + \beta_2 X_2 + \cdots + \beta_n X_n + E \tag{3.10}$$

where $Y = \begin{bmatrix} y_1 \\ y_2 \\ \vdots \\ y_m \end{bmatrix}$, $X_1 = \begin{bmatrix} x_{11} \\ x_{12} \\ \vdots \\ x_{1m} \end{bmatrix}$, $X_2 = \begin{bmatrix} x_{21} \\ x_{22} \\ \vdots \\ x_{2m} \end{bmatrix}$, …, $X_n = \begin{bmatrix} x_{n1} \\ x_{n2} \\ \vdots \\ x_{nm} \end{bmatrix}$, and $E = \begin{bmatrix} \varepsilon_1 \\ \varepsilon_2 \\ \vdots \\ \varepsilon_m \end{bmatrix}$. The method of least squares is used to estimate $\beta_0, \beta_1, \beta_2, \ldots, \beta_n$ by minimizing the residuals. In this case, K^* is assumed to be a product of the powers of three variables—B/H, U/u_*, and λ—and $\exp(a_4\phi_2)$:

$$K^* = a_0 \left(\frac{B}{H}\right)^{a_1} \left(\frac{U}{u_*}\right)^{a_2} \lambda^{a_3} \exp\left(a_4\phi_2\right) \tag{3.11}$$

in which a_0, a_1, a_2, a_3, and a_4 are parameters to be estimated. The different treatment of the secondary flow coefficient anticipates a different dependence; the proposed form becomes 1 when $\phi_2 = 0$. Then, by taking natural logarithm of both sides of Eq. (3.11), the function for K^* can be expressed in the form of Eq. (3.10).

Selection of Data for Regression

Specifying the ranges of the four parameters helps to constrain attempts to develop a formula for the dispersion coefficient. The parameters B/H and U/u_* can be measured during field experiments, and ranges are determined from the experimental data compiled by Nordin and Sabol (1974). The aspect ratio B/H ranges from 16.1 to 266.7, and the parameter U/u_* ranges from 1.5 to 24.2. The median and mean of B/H are 41.8 and 55.9, and the distribution is right-skewed (Figure 1). The median and mean of U/u_* are 6.5 and 8.2, and the distribution is also right-skewed. Because of the skewness, the mean values of both parameters are slightly affected by outliers. Therefore, the medians of B/H and U/u_* are selected as base values.

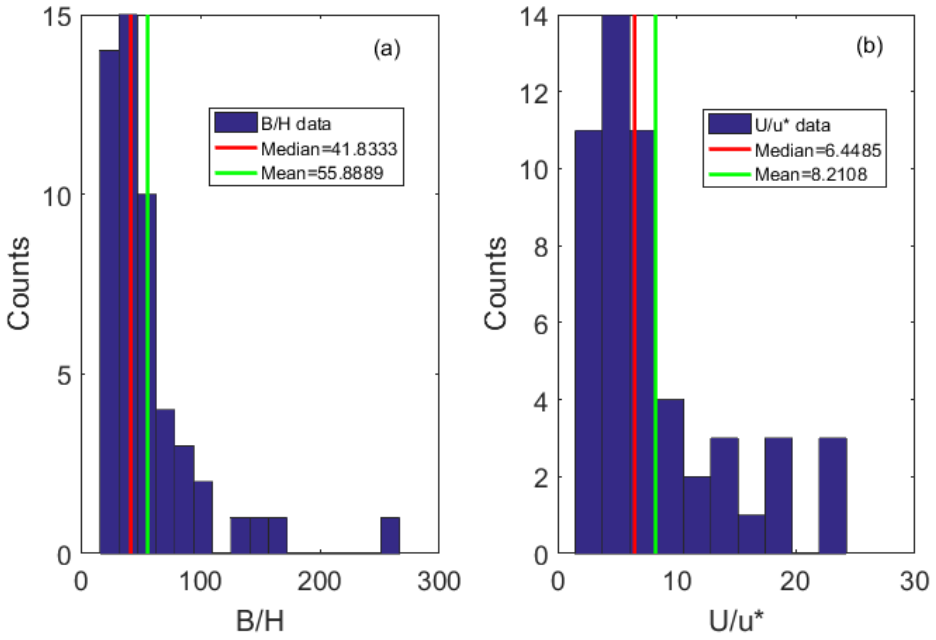

Figure 1. Histograms determined from the data of Nordin and Sabol (1974). (a) B/H; (b) U / u_* .

There are no direct methods to estimate λ and ϕ_2; however, some previous work confines the range of the two parameters. Knight (1999) concluded that the dimensionless transverse eddy viscosity λ is in the range of 0.07−0.5. A parabolic variation of the eddy viscosity, which conforms to the law of the wall, would give a cross sectional average eddy viscosity with λ = 0.067 (Shiono and Knight 1991). Therefore, the base value of λ is set to 0.067. Ervine et al. (2000) indicated that the secondary flow coefficient ϕ_2 is less than 0.5% for straight changes and between 2% and 5% for meandering channels. The base value of ϕ_2 is assumed to be zero; that is, in the base case, no secondary flow occurs.

The base value for each variable (say B/H = 41.8, U / u_* = 6.5, λ = 0.067, and ϕ_2 = 0) is used for observing effective ranges of variables since K* cannot be computed for extreme values of the input variables. After trial and error, five values for each variable were found to confine the ranges of variables (Table 1). There are 5^4 = 625 combinations of these values

included used in the regression analysis. The range matrices of B/H and U/u_* were selected from the data of Nordin and Sabol (1974), and the extreme values were eliminated. Median values are used as the middle value among the ranges in Table 1. Knight (1999) estimated that dimensionless eddy viscosity λ is 0.13 for open channels, 0.16 for a trapezoidal channel, 0.22 for rough floodplains, and 0.27 for smooth floodplains; the value of 0.33 is a moderately high value among the range of 0.07−0.5. Ervine et al. (2000) indicated that the secondary flow coefficient is less than 0.005 for straight rivers and between 0.02 and 0.05 for meandering rivers. Three values of ϕ_2 are chosen for counting the effect of secondary flow on straight channels, and two values are used to explore the meandering channels.

Table 1. Data selection

Variables	B/H	U/u_*	λ	ϕ_2
Range matrix	$\begin{bmatrix}16\\25\\40\\85\\150\end{bmatrix}$	$\begin{bmatrix}3\\5\\7\\12\\18\end{bmatrix}$	$\begin{bmatrix}0.13\\0.16\\0.22\\0.27\\0.33\end{bmatrix}$	$\begin{bmatrix}0\\0.003\\0.005\\0.02\\0.035\end{bmatrix}$

In addition to the values in Table 1, 80 sets in Table 7 in Appendix B are added to stabilize the regression. The stabilization data are assumed to be common data for practical cases: the median value of B/H and U/u_* in the data of Nordin and Sabol (1974) are used for stabilization, and since the triple integration in Eq. (3.7) is derived from the assumption of rectangular channels, a value of 0.13 for λ is selected for stabilization. Two values of ϕ_2 are chosen as 0.005 and 0.02 for representing straight channels and meandering channels. Every

10 sets vary within a selected range of each variable in Table 1 by fixing the other three variables at selected values respectively.

Regression Model Selection

Three parameters are applied to evaluate all types of models: the coefficient of determination R^2, Akaike's information criterion (AIC), and Schwarz's Bayesian criterion (SBC). The coefficient of determination indicates the goodness of fit; higher R^2 occurs for better fits. Smaller values of AIC indicate a preferred model whose expected entropy is maximized (Akaike 1981). A small value of SBC is also preferred for model selection. All possible terms in regression models are summarized in Table 2. X_1–X_4 are the four variables, and X_5–X_{14} are interaction terms between pairs of variables.

Table 2. Terms for selecting a regression model

Terms	Expressions	Terms	Expressions
X_1	$\ln\left(\frac{B}{H}\right)$	X_8	$\ln\left(\frac{B}{H}\right)\cdot\ln\left(e^{\phi_2}\right)$
X_2	$\ln\left(\frac{U}{u_*}\right)$	X_9	$\ln\left(\frac{U}{u_*}\right)\cdot\ln\left(\frac{U}{u_*}\right)$
X_3	$\ln(\lambda)$	X_{10}	$\ln\left(\frac{U}{u_*}\right)\cdot\ln(\lambda)$
X_4	$\ln\left(e^{\phi_2}\right)$	X_{11}	$\ln\left(\frac{U}{u_*}\right)\cdot\ln\left(e^{\phi_2}\right)$
X_5	$\ln\left(\frac{B}{H}\right)\cdot\ln\left(\frac{B}{H}\right)$	X_{12}	$\ln(\lambda)\cdot\ln(\lambda)$
X_6	$\ln\left(\frac{B}{H}\right)\cdot\ln\left(\frac{U}{u_*}\right)$	X_{13}	$\ln(\lambda)\cdot\ln\left(e^{\phi_2}\right)$
X_7	$\ln\left(\frac{B}{H}\right)\cdot\ln(\lambda)$	X_{14}	$\ln\left(e^{\phi_2}\right)\cdot\ln\left(e^{\phi_2}\right)$

Fourteen models, with different numbers of terms, were compared (Table 2). The models including more terms are more accurate since R^2 is larger and AIC and SBC are smaller (i.e., more negative). Wang & Huai (2016) employed only *B/H* as a variable in their model for *K**, and their model is not shown here because *B/H* is not optimal for a one-variable model. The value of R^2 of Model 1, which is the best one-variable model, is much smaller than Model 6 because of missing the consideration of U/u_*, λ, ϕ_2, and interaction terms. In this case, the relations between *K** and all four variables need to be specified; also, the goodness of fit and simplicity of the model should be balanced. Thus, Model 6 is selected for conducting regression analysis. In Model 6, the four variables X_1–X_4 are included, and the two interaction terms, X_9 and X_{11} related to U/u_* and the secondary flow coefficient, are considered. Thus, Model 6 is optimum for conducting regression analysis to estimate the response $Y = \ln(K^*)$. The relationship can be built as

$$Y = \beta_0 + \beta_1 X_1 + \beta_2 X_2 + \beta_3 X_3 + \beta_4 X_4 + \beta_9 X_9 + \beta_{11} X_{11} \tag{3.12}$$

where β_i are the parameters to be estimated with the regression.

Table 3. Comparison of models

Model No.	R-Square	AIC	SBC	Variables in Model
1	0.7092	351.1216	360.21522	X_2
2	0.9138	-494.5006	-480.86028	$X_1\ X_2$
3	0.9747	-1346.2017	-1328.01461	$X_1\ X_2\ X_{11}$
4	0.9819	-1578.3770	-1555.64306	$X_1\ X_4\ X_9\ X_{11}$
5	0.9857	-1740.1204	-1712.83964	$X_1\ X_2\ X_3\ X_4\ X_{11}$
6	0.9879	-1856.7744	-1824.94695	$X_1\ X_2\ X_3\ X_4\ X_9\ X_{11}$
7	0.9885	-1886.4581	-1850.08380	$X_1\ X_2\ X_3\ X_4\ X_9 X_{11}\ X_{13}$
8	0.9888	-1903.2256	-1862.30452	$X_1\ X_2 X_3\ X_4\ X_9\ X_{11}\ X_{13}\ X_{14}$
9	0.9891	-1918.7894	-1873.32157	$X_1\ X_2\ X_3\ X_4\ X_6\ X_9\ X_{11}\ X_{13}\ X_{14}$
10	0.9893	-1932.7698	-1882.75512	$X_1\ X_2\ X_3\ X_4\ X_6\ X_9\ X_{10}\ X_{11}\ X_{13}\ X_{14}$
11	0.9895	-1946.0898	-1891.52834	$X_1\ X_2\ X_3\ X_4\ X_5\ X_6 X_9\ X_{10}\ X_{11}\ X_{13}\ X_{14}$
12	0.9896	-1946.3338	-1887.22562	$X_1\ X_2\ X_3\ X_4\ X_5\ X_6\ X_7\ X_9\ X_{10}\ X_{11}\ X_{13}\ X_{14}$
13	0.9896	-1944.3394	-1880.68438	$X_1\ X_2\ X_3\ X_4\ X_5\ X_6\ X_7\ X_9\ X_{10}\ X_{11}\ X_{12}\ X_{13}\ X_{14}$
14	0.9896	-1942.3410	-1874.13918	$X_1\ X_2\ X_3\ X_4\ X_5\ X_6 X_7\ X_8\ X_9 X_{10}\ X_{11}\ X_{12}\ X_{13}\ X_{14}$

CHAPTER 4. RESULTS AND DISCUSSION

This chapter illustrates the effect of four parameters—the channel aspect ratio, the friction factor, the dimensionless eddy viscosity, and the secondary flow coefficient—on the velocity profiles and dispersion coefficient and evaluates the new empirical formula for the dispersion coefficient. The influence of the four variables on the velocity profiles and longitudinal dispersion coefficient are interpreted, and the results of the regression analysis contributing to the model selection for K^* are presented. The new model is evaluated with laboratory data and measurements from natural rivers, and it is compared with other models to assess its performance.

Velocity Profiles

The velocity profiles give insight into the effect of the four parameters on the dispersion coefficient because the dispersion coefficient is computed from the dimensionless velocity deviation $\hat{u}'$, as Eq. (3.7) shows. The uniformity of velocity profile largely influences K: if the velocity profile is more uniform, the deviation of dimensionless velocity from cross-sectional average will become less, and the dispersion coefficient will be less as well.

The following figures, Figure 2 to 5, show the effects of B/H, U/u_*, λ, and ϕ_2 on the velocity profiles. Each figure varies one variable and sets the other three variables to the base values. The base values of B/H and U/u_* are chosen as 41.83 and 6.45, respectively, the median values from the data of Nordin and Sabol (1974); λ is fixed at 0.067, which is the cross-sectional average from the law of the wall; and ϕ_2 is set as 0, which represent the case

of no secondary flow. In each figure, the black line shows the velocity profile at base values of four variables, and the red and blue lines are comparison groups.

The velocity profile becomes more uniform as the aspect ratio *B/H* increases (Figure 2). Away from the banks, both the term representing the divergence of the turbulent flux and the secondary flow term in the momentum equation (Eq.(3.2)) become small compared to the other terms as *B*/*H* increases. A scaling analysis of the momentum equation can explain the importance of its terms as a function of *B/H*. The main balance is between the bottom shear stress and the *x*-component of the weight. Away from the banks, the ratio of the divergence of the turbulent flux and the bottom shear stress is

$$\frac{\text{divergence of the turbulent flux}}{\text{bottom shear stress}} = \frac{\dfrac{\partial}{\partial y}\left[\rho\lambda H^2\left(\dfrac{f}{8}\right)^{1/2} u\dfrac{\partial u}{\partial y}\right]}{\dfrac{1}{8}\rho f u^2} \sim \frac{\lambda}{f^{1/2}}\left(\frac{B}{H}\right)^{-2} \tag{4.1}$$

As *B*/*H* increases with a constant velocity (or in other words, *f* is an independent fixed value), the divergence of the turbulent flux decreases in importance. Near the banks (for $y \sim \delta$, say), a balance between the divergence of the turbulence flux and bottom shear stress gives an estimate for the dimensionless boundary layer thickness δ / B:

$$\frac{\delta}{B} = \lambda^{1/2}\left(\frac{8}{f}\right)^{1/4}\left(\frac{B}{H}\right)^{-1} \tag{4.2}$$

Eq. (4.2) shows that the dimensionless boundary layer decreases as *B/H* increases if *f* is fixed. Away from the banks the secondary flow term relative to the bottom shear stress is

$$\frac{\text{secondary flow}}{\text{bottom shear stress}} = \frac{\rho\dfrac{\partial}{\partial y}(H\phi_2 u^2)}{\dfrac{1}{8}\rho f u^2} \sim \frac{\phi_2\left(\dfrac{B}{H}\right)^{-1}}{\left(\dfrac{f}{8}\right)} \tag{4.3}$$

Increased *B*/*H* causes the importance of secondary flow to decrease at a given velocity. These results satisfy intuition: One would expect the effects of the banks to decrease as the channel widens. Because the velocity profile is more uniform with increasing *B*/*H*, the dimensionless dispersion coefficient would become smaller as well.

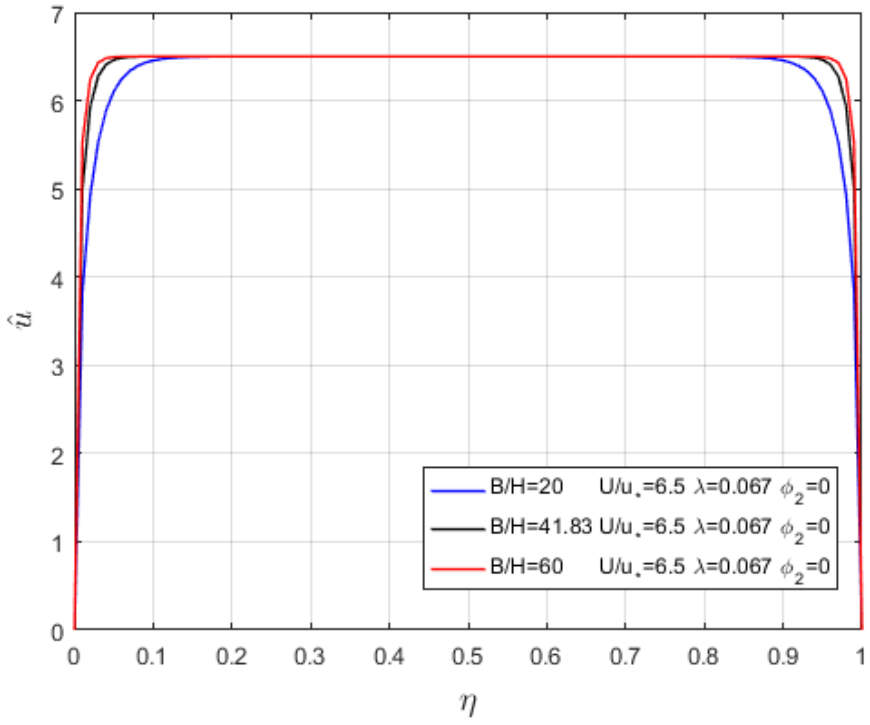

Figure 2. Effect of B/H *on the velocity profile*

Although *B*/*H* does not affect the peak value of the velocity, the friction factor does (Figure 3). The peak velocity increases as the friction factor decreases, or U/u_* increases, as shown in Eq. (3.5). Away from the banks, the main balance in the momentum equation [Eq. (3.2)] is between the first two terms: the *x*-component of the weight (per unit volume) and the bottom shear stress. This balance gives

$$u \approx \sqrt{\frac{8gHS_0}{f}} \quad \text{or} \quad \hat{u} = \sqrt{\frac{8}{f}} = \frac{U}{u_*} \tag{4.4}$$

For a smaller friction factor *f*, a larger velocity is needed to balance the gravitational component in the streamwise direction. Also, as shown above, a larger friction factor (or smaller value of U/u_*) decreases the width of the boundary layer, which confirms the boundary layer thickness δ below:

$$\delta = \frac{u}{\sqrt{gHS_0}} \lambda^{1/2} H \left(\frac{f}{8}\right)^{1/4} = \frac{U}{u_*} \lambda^{1/2} H \left(\frac{f}{8}\right)^{1/4} = \lambda^{1/2} H \left(\frac{f}{8}\right)^{-1/4} \tag{4.5}$$

Therefore, because the velocity profile becomes less uniform as U/u_* increases, the dimensionless dispersion coefficient would be expected to increase with U/u_* as well.

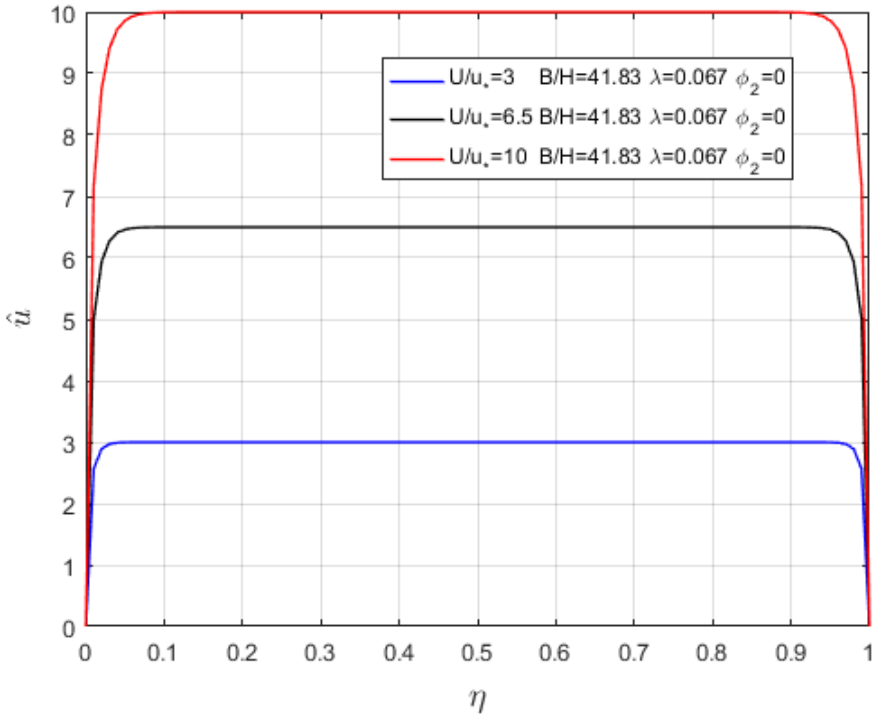

Figure 3. Effect of U/u_* on the velocity profile

Over the range of typical values, the dimensionless eddy viscosity has little effect on the velocity profile (Figure 4). As with *B*/*H*, Eq. (4.4) shows that λ does not affect the peak velocity; the effects of the dimensionless eddy viscosity are confined to the boundary layers

near the banks. The uniformity of the velocity profile slightly decreases with an increase of λ. As shown in Eq. (4.5), the boundary layer thickness for zero or small secondary flow is proportional to $\lambda^{1/2}$, so a factor of 7.5 change in λ results in a boundary layer that is 2.5 times larger. These results indicate that the dimensionless dispersion coefficient should increase as the dimensionless eddy viscosity increases, though perhaps not strongly.

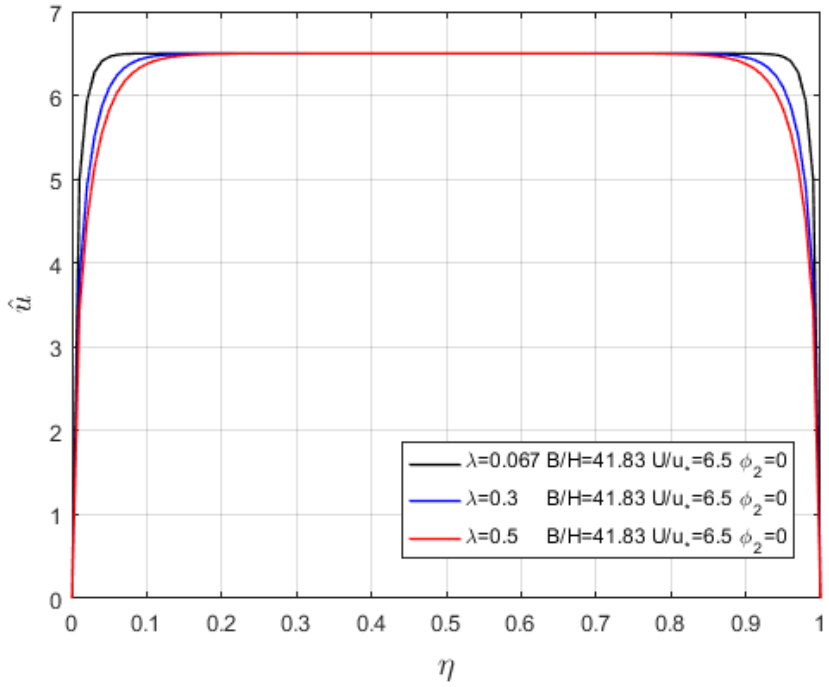

Figure 4. Effect of the dimensionless eddy viscosity on the velocity profile

The secondary flow coefficient affects not only the symmetry of the profiles but also the size of the boundary layer (Figure 5). When no secondary flow is present ($\phi_2 = 0$), the velocity profile is symmetric, and as ϕ_2 becomes positive and larger, the profiles become more skewed toward the right bank. Unlike the other three parameters, ϕ_2 affects the thicknesses of the boundary layers on the left and right banks differently: As ϕ_2 increases, the boundary layer on the left widens, while the boundary layer on the right contracts. Because the boundary layer thickness is inversely proportional to $r_{1,2}$, and r_2, a smaller root of the

linear differential equation, leads to a larger boundary layer on the left; in contrast, the larger root r_1 induces a smaller boundary layer on the right. In the special case of no secondary flow (Figures 2, 3 and 4), the velocity profiles are symmetrical since the absolute values of r_1 and r_2 are equal in Eq. (3.4). Overall, the uniformity of velocity profile decreases with increasing secondary flow coefficient, and dispersion coefficient is expected to increase with more secondary flow.

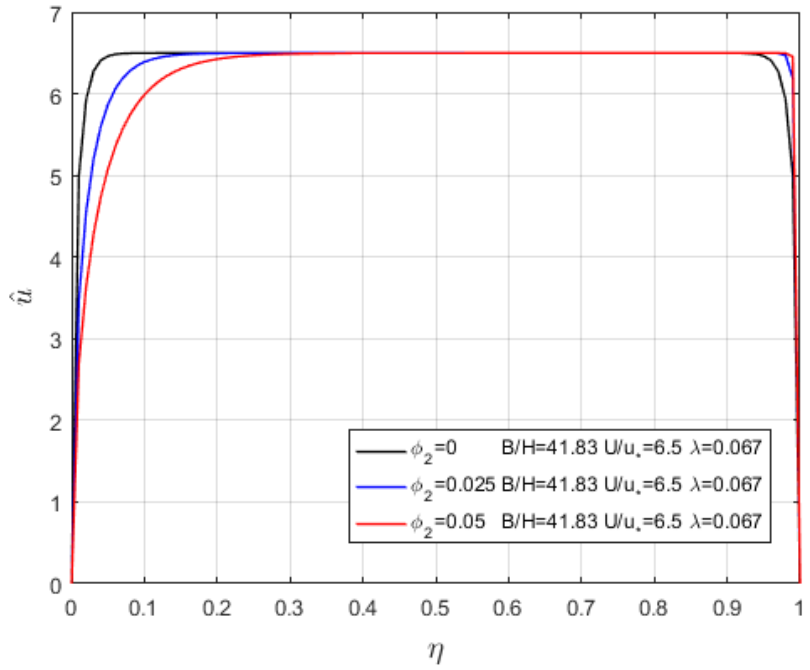

Figure 5. Effect of the secondary flow coefficient ϕ_2 on the velocity profile

Dimensionless Dispersion Coefficient

The variation of the dimensionless dispersion coefficient $K / u_* H$ with the four variables, shown in Figure 6 to 9, is helpful for understanding the dispersion process. From Eq. (3.7), the relation between the dispersion coefficient K and K^* is

$$K = \frac{gHS_0B^2}{D_y} K^* \tag{4.6}$$

and the dispersion coefficient is normalized by u_*H

$$\frac{K}{u_*H} = \frac{gHS_0B^2}{D_y u_*H} K* \tag{4.7}$$

recall that $D_y = D_{y0}u_*H$ and $u_* = \sqrt{gRS_0} = \sqrt{g\frac{BH}{B+2H}S_0}$ for a rectangular channel. The dimensionless dispersion coefficient is

$$\frac{K}{u_*H} = \frac{1}{D_{y0}}\left(\frac{B}{H}\right)\left(\frac{B}{H}+2\right)K* \tag{4.8}$$

The dimensionless dispersion coefficient K^* is calculated by Matlab, and D_{y0} is obtained by Eq. (2.15).

The black stars in Figure 6 to 9 are at the base values in order to compare how other three variables affect the univariate figures. As in the previous subsection, *B/H* and U/u_* are fixed at 41.83 and 6.45, respectively, the median values from Nordin and Sabol (1974), and λ is fixed at 0.067, the average assuming the law of the wall holds, and the secondary flow coefficient ϕ_2 is fixed at zero, which means no secondary flow occurs.

The dimensionless dispersion coefficient varies non-monotonically with *B*/*H* (Figure 6). The base group indicates that K/u_*H decreases with *B/H* in the range 15 < *B*/*H* < 70 and increases with *B*/*H* for larger values. When λ is increased to 0.3 in the green star group, the region of decreasing K/u_*H extends to *B/H* = 160. As the secondary flow coefficient and U/u_* change for the blue and red star groups respectively, the slopes of *B/H* change as well. The change of slope indicates that the variation of K/u_*H with *B/H* is related to the other three variables, yet the higher value of U/u_* contributes to stabilize the slope change since the slope of red group shifts to be positive as U/u_* decreases to 3. Also, when *B/H* is more

than 200, K/u_*H of the green star group is close to that of the base value group, which implies that when *B/H* is large, the influence of dimensionless eddy viscosity on dimensionless dispersion is not as strong as the case that *B/H* is less than 100.

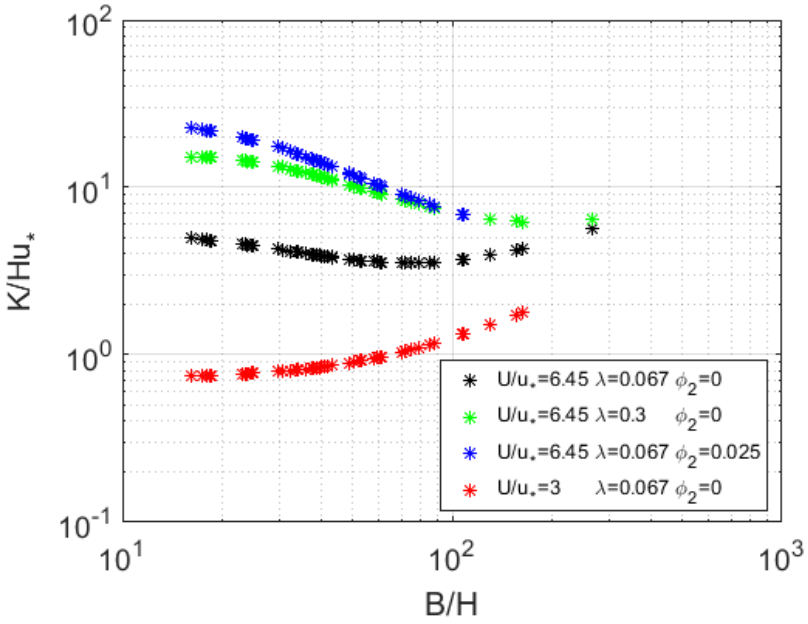

Figure 6. Effect of B/H on the dimensionless dispersion coefficient

For the values of parameters considered in Figure 7, K/u_*H always increases with U/u_*. With no secondary flow ($\phi_2 = 0$), K/u_*H is linearly proportional to U/u_* on the log-log plot; in fact the dimensionless dispersion coefficient follows an approximately linear relation. The green and blue star groups are parallel to the base value group, which means that changing *B/H* and λ does not alter the variation of K/u_*H with U/u_*. After $U/u_* = 20$, the slope of the red star group increases, which indicates that secondary flow influences the variation of K/u_*H with U/u_*. From Eq. (4.3), the secondary flow term in the momentum equation is important when

$$\phi_2 \sim \frac{f}{8}\frac{B}{H} = \left(\frac{U}{u_*}\right)^{-2}\left(\frac{B}{H}\right) \tag{4.9}$$

The influence of U/u_* on the effect of secondary flow is large since the term has an exponent of −2 compared to the term involving *B/H*; in other words, when U/u_* is large, secondary flow can have significant impact.

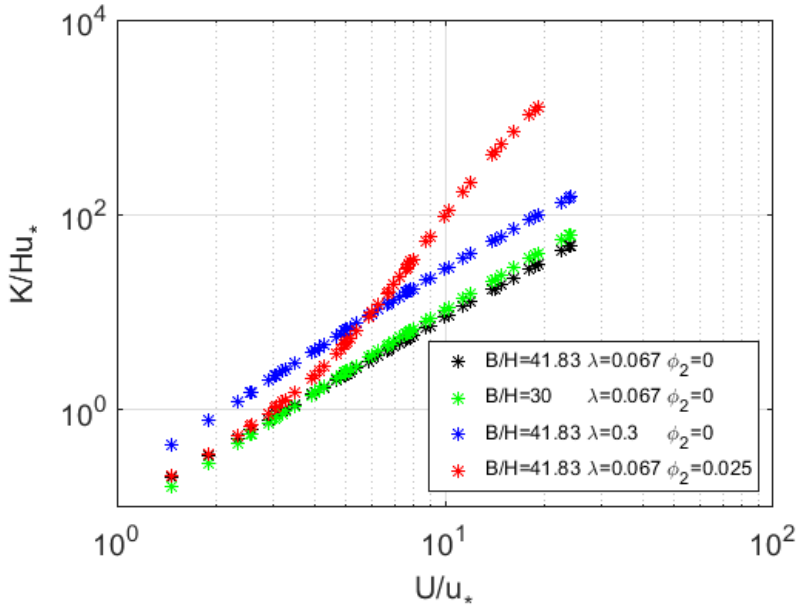

Figure 7. Effect of U/u_* on the dimensionless dispersion coefficient

The dimensionless dispersion coefficient also follows a power law with dimensionless eddy viscosity (Figure 8). Both the red and green star groups are parallel to the base group. Therefore, the variation of K/u_*H with dimensionless eddy viscosity is not affected by *B/H* and U/u_*. By increasing secondary flow coefficient from zero to 0.025, the slope of the blue star group decreases, which means secondary flow coefficient influences the relation between K/u_*H and λ.

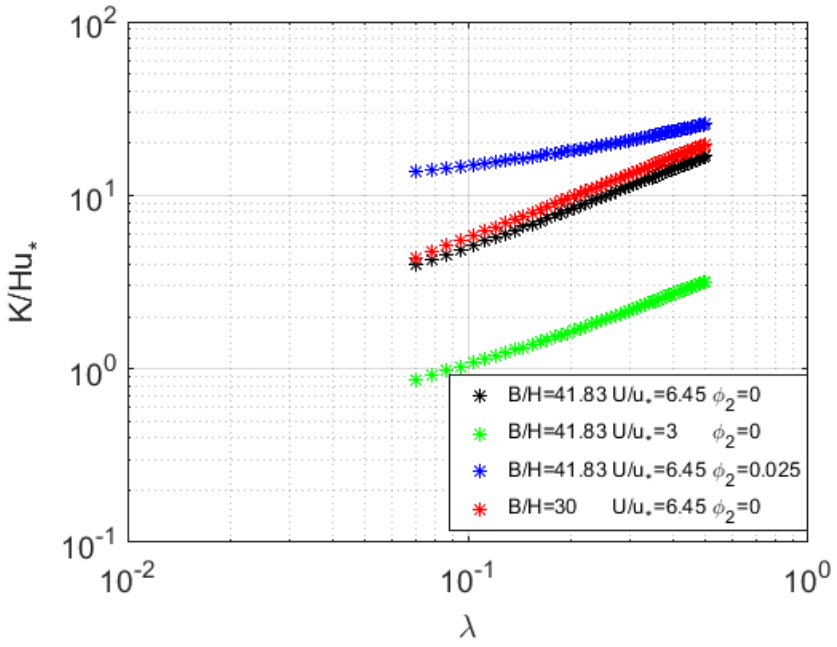

Figure 8. Effect of dimensionless eddy viscosity on dimensionless dispersion coefficient

The results in Figure 9 reflect the balance of terms in the momentum equation, Eq. (3.2). Plotting against exp(ϕ_2) anticipates the empirical relation because that factor is one when no secondary flow exists. As the analysis of velocity profiles suggests, the dimensionless dispersion coefficient increases as secondary flow becomes stronger. A comparison of the last two terms in the momentum equation gives

$$\frac{\text{secondary flow term}}{\text{divergence of turb. flux}} = \frac{\rho \dfrac{\partial}{\partial y}(H\phi_2 u^2)}{\dfrac{\partial}{\partial y}\left[\rho\lambda H^2\left(\dfrac{f}{8}\right)^{1/2} u\dfrac{\partial u}{\partial y}\right]} \sim \frac{\phi_2}{\lambda}\frac{B}{H}\left(\frac{8}{f}\right)^{1/2} = \frac{\phi_2}{\lambda}\frac{B}{H}\left(\frac{U}{u_*}\right) \tag{4.10}$$

Eq. (4.10) shows that when

$$\phi_2 > \lambda\left(\frac{B}{H}\right)^{-1}\left(\frac{U}{u_*}\right)^{-1} \tag{4.11}$$

the secondary flow is significant. That is, secondary flow becomes more important as U / u_* increases; *B/H* increases, or λ decreases. These results can be seen by comparing the red, the blue, and green star curves to the base group, denoted by the black curve.

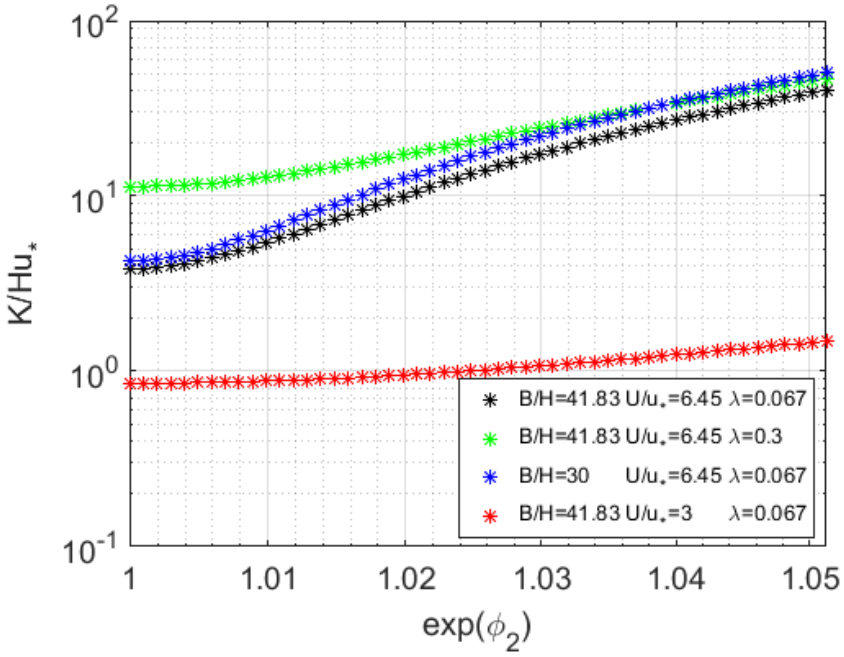

Figure 9. Effect of the secondary flow coefficient, expressed as e^{ϕ_2} , on the dimensionless dispersion coefficient

The results for the dimensionless dispersion coefficient give insight into the empirical formula to be developed: 1) the dimensionless dispersion coefficient does not depend on the four variables in isolation; their effects can combine; 2) the secondary flow coefficient affects the variation of the dimensionless dispersion coefficient on the other three variables; and 3) U / u_* has the largest influence on the magnitude of the dimensionless dispersion coefficient.

Development of the New Model for *K**

Regression Assessment

Based on the numerical calculations, Figure 10 shows that there are approximate linear relations between $\ln(K^*)$ and $\ln\left(\frac{U}{u_*}\right)$, $\ln\left(\frac{B}{H}\right)$, $\ln(\lambda)$, $\ln\left(e^{\phi_2}\right)$, $\left(\ln\left(\frac{U}{u_*}\right)\right)^2$, and $\ln\left(\frac{U}{u_*}\right)\cdot\ln\left(e^{\phi_2}\right)$. Therefore, the regression method can be used to specify the relations between *K** and the four variables, as well as the interaction terms.

In Figure 10, the ranges of *B/H* and U/u_* are from the data of Nordin and Sabol (1974); the dimensionless eddy viscosity varies within the range of 0.07 to 0.5 (Shiono 1999); the secondary flow coefficient falls in the range of 0 to 0.05 (Ervine et al. 2000). The figures are plotted based on similar scenarios when analyzing the dimensionless dispersion coefficient, say observing the change of one variable by fixing other three variables. Since the variable in Figure 10f is an interaction term involving $\ln\left(e^{\phi_2}\right)$ and $\ln\left(\frac{U}{u_*}\right)$, the comparison groups of ϕ_2 are made. The comparison groups show that changing the value of ϕ_2 does not affect the linear relationship between $\ln(K^*)$ and $\ln\left(e^{\phi_2}\right)$.

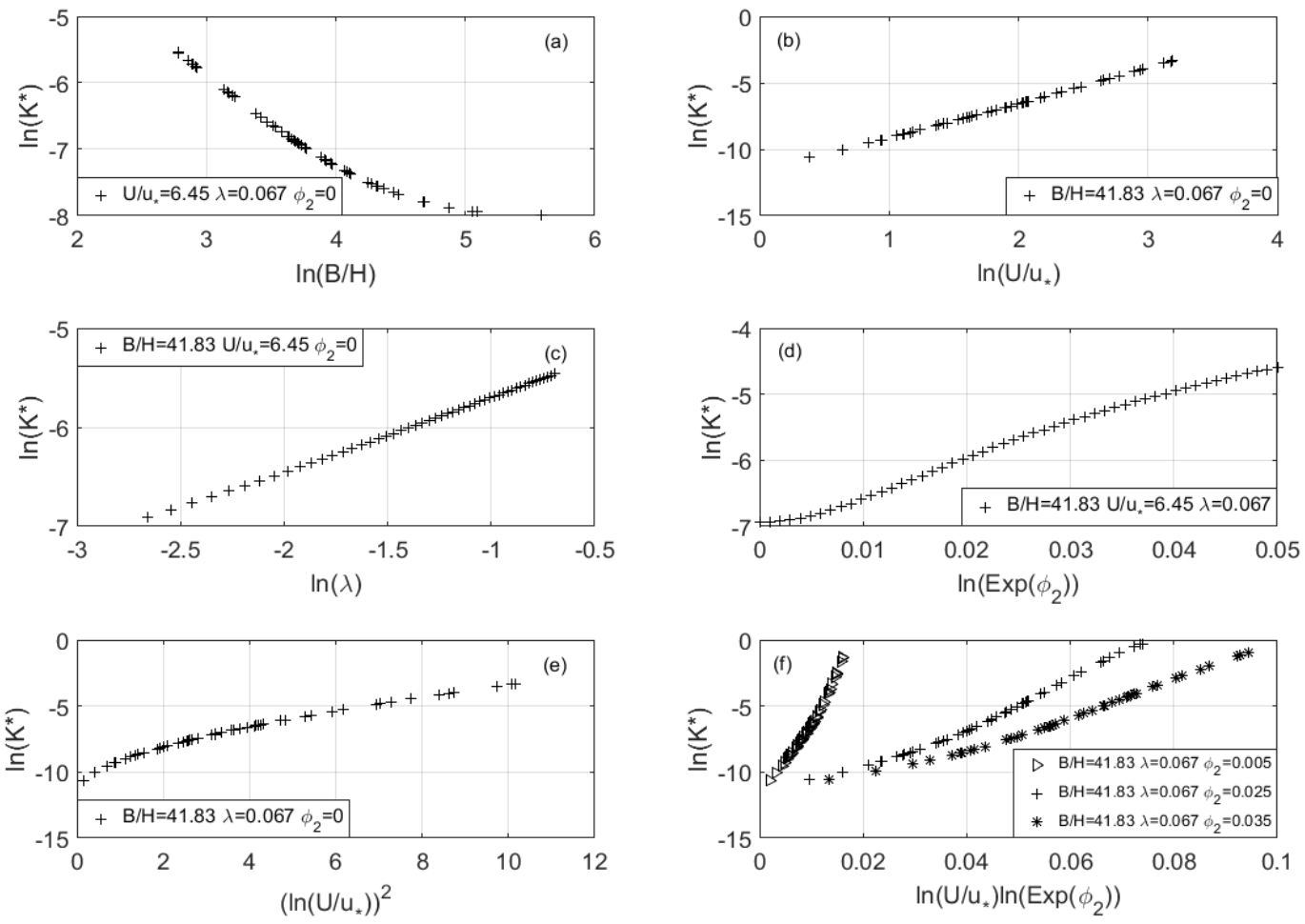

Figure 10. Multiple regression on $\ln(K^*)$ *: (a)* $\ln(K^*)$ *versus* $\ln(B/H)$ *; (b)* $\ln(K^*)$ *versus* $\ln(U/u_*)$ *; (c)* $\ln(K^*)$ *versus* $\ln(\lambda)$ *; (d)* $\ln(K^*)$ *versus* $\ln\left(e^{\phi_2}\right)$ *; (e)* $\ln(K^*)$ *versus* $\ln\left(U/u_*\right)\cdot\ln\left(U/u_*\right)$ *; (f)* $\ln(K^*)$ *versus* $\ln(U/u_*)\cdot\ln\left(e^{\phi_2}\right)$

Regression Analysis

Model 6 is used for regression analysis to obtain an expression for K^*. The relationship can be built as shown in Eq. (3.12). Table 4 shows the values of parameters, β_i. Thus, Eq. (3.12) can be written as:

$$Y = -4.20 + (-1.36)X_1 + 1.4X_2 + 0.44X_3 + (-50.54)X_4 + 0.33X_9 + 46X_{11} \tag{4.12}$$

Inserting the definitions of the model parameters and solving for K^* gives

$$K^* = 0.015\lambda^{0.44} e^{-50.54\phi_2} \left(\frac{B}{H}\right)^{-1.36} \left(\frac{U}{u_*}\right)^{1.4+0.33\ln(U/u_*)+46\phi_2} \tag{4.13}$$

the expression of dimensionless dispersion coefficient is derived as:

$$\frac{K}{u_* H} = \frac{0.015}{D_{y0}} \lambda^{0.44} e^{-50.54\phi_2} \left(\frac{B}{H}\right)^{-0.36} \left(\frac{B}{H} + 2\right) \left(\frac{U}{u_*}\right)^{1.4+0.33\ln(U/u_*)+46\phi_2} \tag{4.14}$$

where D_{y0} is defined in Eq. (2.15) and is related to the transverse mixing coefficient.

Table 4. Parameter estimates

Parameter Estimates							
Variable	**DF**	**Parameter Estimate**	**Standard Error**	**t Value**	**Pr > |t|**	**95% Confidence Limits**	
Intercept	1	-4.19682	0.13235	-31.71	<.0001	-4.45668	-3.93696
X_1	1	-1.35955	0.01295	-105.00	<.0001	-1.38497	-1.33413
X_2	1	1.40479	0.12101	11.61	<.0001	1.16721	1.64238
X_3	1	0.43973	0.02856	15.40	<.0001	0.38365	0.49581
X_4	1	-50.54427	2.67543	-18.89	<.0001	-55.79723	-45.29131
X_9	1	0.33419	0.02953	11.32	<.0001	0.27620	0.39217
X_{11}	1	46.00017	1.29442	35.54	<.0001	43.45870	48.54164

Because the p-value is less than the level of significance, which defaults as 0.05, the null hypothesis is rejected. In other words, $X_1 - X_4$, X_9, and X_{11} can be modeled by multiple

regression. The t-statistics are given by the ratio of parameter estimate to standard error, and the 95% confidence intervals can be obtained based on the t-value.

The analysis of variance for Model 6 is summarized in Table 5. There are 705 sets data in total, and 696 sets are used for regression analysis. Mean squared error (MSE) is 0.069. Since the p-value is less than the level of significance 0.05, the null hypothesis, which is $\beta_1 = \beta_2 = \beta_3 = \beta_4 = \beta_9 = \beta_{11} = 0$, is rejected; therefore, Model 6 is useful for estimating K^*. The coefficient of determination R^2 for Model 6 is 98.79%.

Table 5. Analysis of variance (ANOVA)

Analysis of Variance					
Source	**DF**	**Sum of Squares**	**Mean Square**	**F Value**	**Pr > F**
Model	6	3896.02407	649.33735	9413.47	<.0001
Error	690	47.59594	0.06898		
Corrected Total	696	3943.62001			

The previous section indicates the variables are not independently related to dimensionless dispersion coefficient. This model confirms observations from Figure 7 and Figure 9: U / u_* and the secondary flow coefficient have significant interactive influence on the dimensionless dispersion coefficient.

Evaluation of the New Model

The new model Eq. (4.14) is assessed in this section by using data from the laboratory experiments of Perucca et al. (2009) and Wang & Huai (2016) shown in Table 6 and plotted in Figure 11. Both research groups conducted experiments for flows in straight rectangular channels, for which D_{y0} is 0.15. Neither research group estimated values of λ and ϕ_2. However, the values can be estimated based on previous work. Shiono and Knight (1991) indicated that λ is 0.13 for open channels, and that value is adopted here. Ervine et al. (2000) found that ϕ_2 is less than 0.5% if a channel is straight and between 2%-5% when a channel is meandering. Because secondary flow coefficient is related to the transverse mixing coefficient (Deng et al. 2001), an estimate for ϕ_2 is

$$\phi_2 = 0.05\frac{D_{y0} - 0.145}{0.6 - 0.145} = 0.11\left(D_{y0} - 0.145\right) \tag{4.15}$$

where the values of 0.145 and 0.6 are the lower and upper bounds of D_{y0} respectively from Fischer et al. (1979). Once D_{y0} is computed with Eq. (2.15) ϕ_2 can be computed with Eq. (4.15).

Table 6. Comparison with lab experiment data. The channel slope is 0.00075 for the study of Perucca et al. (2009) and 0.0004 for the study of Wang & Huai (2016). The Manning roughness coefficient is 0.01 for both.

Research Group	B (m)	H (m)	U (m/s)	u_* (m/s)	K_{tracer} (m^2/s)	K_{new1} (m^2/s) Eq.(4.14)
Perucca et al. (2009)	0.44	0.035	0.104	0.016	0.01	0.00539
	0.44	0.04	0.188	0.017	0.017	0.03382
	0.44	0.053	0.232	0.02	0.032	0.05152
	0.44	0.05	0.136	0.019	0.006	0.01042
	0.44	0.068	0.144	0.022	0.013	0.01143
	0.44	0.082	0.166	0.025	0.035	0.01532
	0.44	0.065	0.087	0.022	0.01	0.00313
Wang & Huai (2016)	1	0.12	0.11	0.022	0.0137	0.01086
	1	0.14	0.118	0.023	0.0165	0.01344
	1	0.16	0.125	0.025	0.0219	0.01500
	1	0.18	0.133	0.027	0.0254	0.01965
	1	0.2	0.14	0.028	0.0239	0.02356

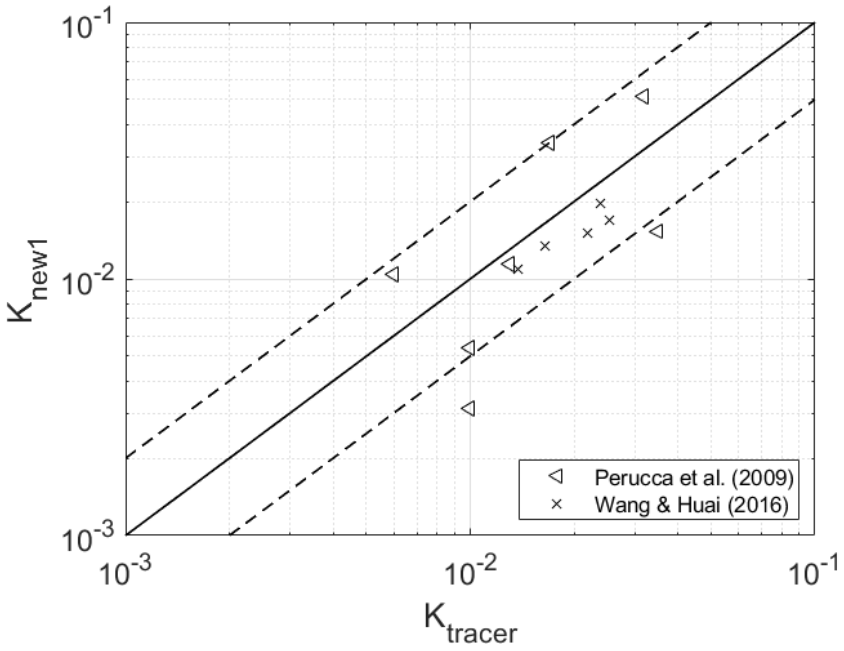

Figure 11. Comparison of K_{new1} in Eq.(4.14) *and tracer study measurements. The solid line shows the case in which K_{new1} is equal to K_{tracer}; the two dashed lines bound the range of $0.5<K_{new1}/K_{tracer}<2$.*

The new formula predicts dispersion coefficients from laboratory experiments well (Figure 11). Nine of the twelve estimates from K_{new1} fall in the range of $0.5 < K_{new1}/K_{tracer} < 2$, and only two estimates—all from the data of Perucca et al. (2009)—have comparatively large error. K_{new1} estimates perform better with the experimental results of Wang & Huai (2016). The discrepancy ratio in Eq. (2.13) is employed to assess the accuracy of K_{new1} more quantitatively.

$$\mathrm{DR(new1)} = \log_{10}\left(\frac{K_{new1}}{K_{tracer}}\right) \tag{4.16}$$

The mean of DR(new1) is -0.088, and the median is -0.095. The overall estimates from K_{new1} tend to be slightly underestimated but still in a reasonable range (e.g., the standard deviation is 0.24), and both the mean and median values of DR(new1) are close to zero, where K_{new1} is equal to K_{tracer},

To be used in predicting dispersion coefficients in natural channels, the estimates need to be adjusted. When K_{new1} is applied to the data of Nordin and Sabol (1974), the dispersion coefficients are underestimated by two orders of magnitude. As noted in chapter 2, Deng et al. (2001) and Wang and Huai (2016) made similar adjustments to their formulas, which were derived for straight channels with smooth banks. Since the model of Wang and Huai (2016) and the new model are based on the momentum equation (Shiono and Knight 1991) and the dispersion coefficient solution in Eq. (2.1), a relationship between K_1 in Eq. (2.23) from Wang and Huai (2016) and K_{new1} is expected (Figure 12). The model of Wang and Huai (2016) is defined as $\frac{K_1}{u_* H} = 0.0798\left(\frac{B}{H}\right)^{0.6239}\left(\frac{U}{u_*}\right)^2$, which is derived from building an univariate model for *B/H* to estimate the triple integral in Eq. (2.1).

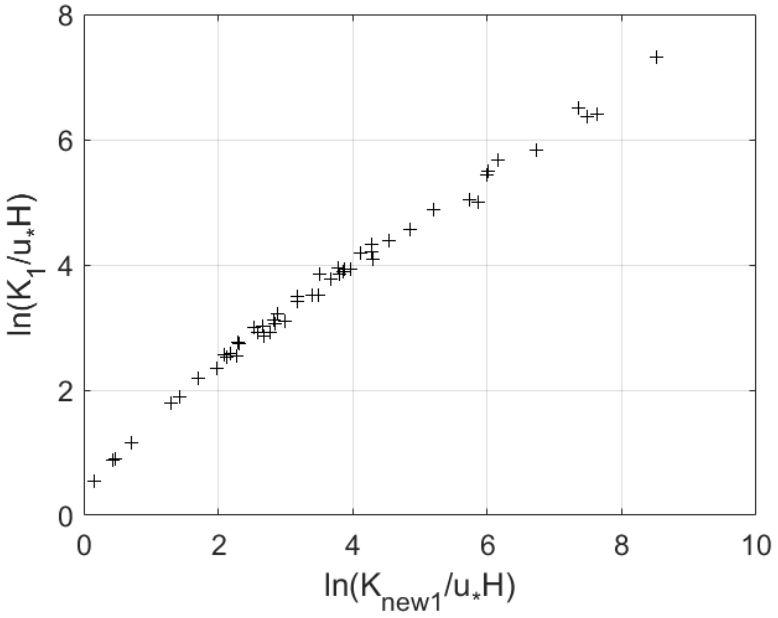

Figure 12. $\ln(\frac{K_{new1}}{u_* H})$ *versus* $\ln\left(\frac{K_1}{u_* H}\right)$

In Figure 12, the relation between K_1 estimated from Wang and Huai and K_{new1} is

$$\ln\left(\frac{K_1}{u_* H}\right) = 0.7655 \ln\left(\frac{K_{new1}}{u_* H}\right) + 0.9587 \qquad R^2 = 0.9888 \tag{4.17}$$

Then plugging Eq. (4.17) into Eq. (2.23) to get $\ln\left(\frac{K_2}{u_* H}\right)$, and in this case

$$\ln\left(\frac{K_2}{u_* H}\right) = \ln\left(\frac{K_{new2}}{u_* H}\right) \tag{4.18}$$

A new revision model is built:

$$\ln\left(\frac{K_{new2}}{u_* H}\right) = 0.4451 \ln\left(\frac{K_{new1}}{u_* H}\right) + 4.821 \tag{4.19}$$

and the form of Eq.(4.19) can be changed into

$$\frac{K_{new2}}{u_* H} = \frac{19.14}{(D_{y0})^{0.4451}} \left(\frac{B}{H}\right)^{-0.16} \left(\frac{B}{H} + 2\right)^{0.45} \left(\frac{U}{u*}\right)^{0.62+0.15\ln\left(\frac{U}{u_*}\right)+20.47\phi_2} \lambda^{0.2} e^{-22.5\phi_2} \qquad (4.20)$$

K_{new2} is the revised model of K_{new1} for calculations for natural rivers,

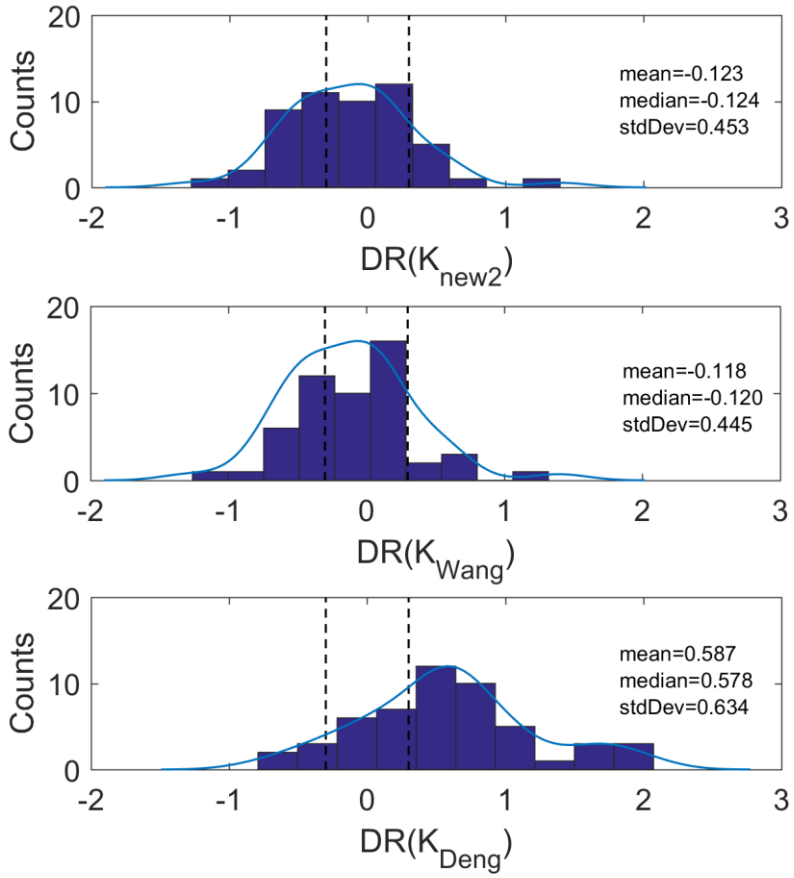

Figure 13. Comparison of models for the dispersion coefficient for natural rivers; the two dash lines bound the range of $0.5 < K_{predicted} / K_{tracer} < 2$.

The revised model in Eq. (4.20) is evaluated with the data from Nordin and Sabol (1974) and compared with the models of Deng et al. (2001) and Wang and Huai (2016) in Figure 13. The secondary flow coefficient ϕ_2 is estimated from Eq. (4.15), and dimensionless eddy viscosity is set to be 0.27 for smooth floodplain (Shiono 1999). The three models are selected because all three are based on Taylor's shear dispersion theory. Eq. (4.20) and the

model of Wang & Huai (2016) produce similar results; both models underestimate slightly on average because the mean and median of both models are −0.12. The standard deviations of both models are less than half an order of magnitude. The predictions of Deng et al. (2001) tend to overestimate by about half an order of magnitude.

Summary

Examining how the velocity profiles and dimensionless dispersion coefficient vary with the aspect ratio, friction factor, dimensionless eddy viscosity, and secondary flow coefficient shows that the variation with each variable cannot be isolated. Therefore, a model with appropriate interaction terms is selected, and regression analysis is used to obtain K_{new1}, an expression for the dispersion coefficient. Applied to laboratory data, the expression predicts 83.3% of the results within a factor of 2—that is, $0.5 < K_{new1}/K_{tracer} < 2$. However, K_{new1} underestimates dispersion for natural rivers since the environmental conditions are more complicated than lab conditions. Therefore, K_{new1} is adjusted using the revision model from Wang and Huai (2016). The new expression K_{new2} performs better than the model of Deng et al. (2001) model about as well as the model of Wang and Huai (2016).

CHAPTER 5. CONCLUSION

This research aimed to provide better estimates for the dispersion coefficient with limited information, such as knowing *B/H* and U / u_* only. By utilizing the observed ranges of secondary flow coefficient (e.g., relating the secondary flow coefficient to the transverse mixing coefficient) and certain values of dimensionless eddy viscosity (say λ = 0.067, 0.13, and 0.27 for the boundary layer, open channel, and smooth floodplain, respectively), the dispersion coefficient can be justified with two more factors for improving the accuracy of the estimation. The expression for *K* is developed using the shear dispersion theory of Taylor (1954) and the momentum equation presented by Shiono and Knight (1991). Multiple regression is used to relate the dimensionless dispersion coefficient *K** to *B*/*H*, U / u_*, the dimensionless eddy viscosity λ, and the secondary flow coefficient ϕ_2, and an appropriate model is selected with two interaction terms, involving U / u_* and e^{ϕ_2}. Thus, the initial model K_{new1} is estimated. The initial model fits the experiments results conducted by Perucca et al. (2009) and Wang & Huai (2016) well: 83.3% of the experimental results are predicted within the range $0.5 < K_{new1}/K_{tracer} < 2$. However, an adjustment needs to be made since the initial model underestimates the dispersion coefficient for natural channels. By using the revision model provided by Wang and Huai (2016), the second model K_{new2} is obtained. The performance of K_{new2} for natural rivers is better than the model of Deng et al. (2001), and it is as good as the model produced by Wang & Huai (2016), which is tested to be relatively accurate with the data of Nordin and Sabol (1974).

REFERENCES

Bogle, G. V. (1997). “Stream velocity profiles and longitudinal dispersion.” *J. Hydraul. Eng.*, 123, 816-820.

Akaike, H. (1981). “Likehood of a model and information criteria.” *J. Econometrics*, 16, 3-14.

Carr, M. L., and Rehmann, C. R. (2007). “Measuring the dispersion coefficient with acoustic Doppler current profilers.” *J. Hydraul. Eng.*, 133(8), 977–982.

Deng, Z. Q., Singh, V. P., and Bengtsson, L. (2001). “Longitudinal dispersion coefficient in straight rivers.” *J. Hydraul. Eng.*, 127(11), 919–927.

Elder, J. W. (1959). “The dispersion of marked fluid in turbulent shear flow.” *J. Fluid Mech.*, 5(4), 544–560.

Ervine, D. A., Babaeyan-Koopaei, K., and Sellin, R. H. J. (2000). “Two-dimensional solution for straight and meandering overbank flows.” *J. Hydraul. Eng*., 126(9), 653–669.

Fischer, H. B. (1967). “The mechanics of dispersion in natural streams.” *J. Hydraul. Div. ASCE*, 93(6), 187–216.

Fischer, H. B., List, E. J., Koh, R. C. Y., Imberger, J., and Brooks, N. H. (1979). *Mixing in Inland and Coastal Waters*, Elsevier, New York.

Jobson, H. E. (1996). “Prediction of traveltime and longitudinal dispersion in rivers and streams.” USGS Water-Resources Investigations Report 96-4013.

Kashefipour, S. M., and Falconer, R. A. (2002). “Longitudinal dispersion coefficients in natural channels.” *Water Res.*, 36(6), 1596–1608.

Knight, D. W. (1999). “Flow mechanisms and sediment transport in compound channels.” *Int. J. Sed. Res.*, 14(2), 217–236.

Nordin, C. F., and G. V. Sabol (1974). “Empirical data on longitudinal dispersion in rivers.” U.S. Geological Survey, Water-Resources Investigations, 332, 20-74.

Rutherford, J. C. (1994). *River Mixing*. Chichester, UK: John Wiley and Sons Ltd.

Perucca, E., Camporeale, C., and Ridolfi, L. (2009). “Estimation of the dispersion coefficient in rivers with riparian vegetation.” *Adv. Water Resour.*, 32(1), 78–87.

Samuels, W. B., Bahadur, R., Ziemniak, C., and Amstutz, D. E. (2015). “Development and application of the incident command tool for drinking water protection.” *Water Environ. J.*, 29(1), 1–15.

Seo, W., and Cheong, Tae, S. (1998). “Predicting longitudinal dispersion coefficient in natural streams.” *J. Hydraul. Eng*., 124(1), 25–32.

Shen, C., J. Niu, E. J. Anderson & M. S. Phanikumar (2010). “Estimating longitudinal dispersion in rivers using Acoustic Doppler Current Profilers.” *Adv. Water Resour.*, 33, 615-623.

Shiono, K., and Knight, D. W. (1988). “Two-dimensional analytical solution for a compound channel.” *Proc., 3rd Int. Symp. on Refined Flow Modelling and Turbulence Measurements*, Tokyo, 503–510.

Shiono, K., and Knight, D. W. (1991). “Turbulent open-channel flows with variable depth across the channel.” *J. Fluid Mech.*, 222, 617–646.

Taylor, G. (1953). “Dispersion of soluble matter in solvent flowing slowly through a tube.” *Proc. R. Soc. London A: Math. Phys. Eng. Sci.*, 219(1137), 186–203.

Taylor, G. (1954). “The dispersion of matter in turbulent flow through a pipe.” *Proc. R. Soc. London A: Math. Phys. Eng. Sci.*, 223(1155), 446–468.

Wang, Y., and Huai, W. (2016). “Estimating the longitudinal dispersion coefficient in straight natural rivers.” *J. Hydraul. Eng.*, 142(11), 1–11.

APPENDIX A MATLAB CODES

*K** calculation

```
% Oct. 5, 17
% Yuqi Song
% Data Input for Kstar Calculation

    clear; close all

    % read data
    [NSdata] = xlsread('C:\Users\Yuqi
Song\Desktop\Thesis\Thesis\NSdata.xlsx','Sheet3');

    % obtain variables
    w1     = NSdata(:,6)';          % w1   = B/H
    u1     = NSdata(:,7)';          % u1   = U/ustar
    L      = NSdata(:,8)';          % lambda is the lateral dimensionless
eddy viscosity
    Phi_2  = NSdata(:,9)';          % secondary flow coefficient
    f      = 8.*u1.^(-2);           % f is friction factor;
    g      = 9.8;

    % Kstar calculation
    Kstar  = Calcs_K_Function(w1,f,L,phi_2);        % K*
```

Calcs_K_Function

```
function [K] = Calcs_K_Function(w1,f,L,phi_2)


    % Sept. 16, 17
    % Yuqi Song
    % Momentum Method for getting dispersion coefficient

    g  = 9.8;           %  Acceleration of gravity (m/s2)
    ny = 101;           %  Number of points in y


    y = linspace(0,1,ny);

    % r1, r2, A1, A2, wd equations

    r1   = w1./L.*sqrt(8./f).*(phi_2+sqrt(phi_2.^2+L.*f.*sqrt(f./8)./4));

    r2   = 2.*phi_2.*w1./L.*sqrt(8./f)-r1;

    wd   = g*(8./f);

    A1   = (exp(r2)-1)./(exp(r1)-exp(r2));
```

```
    A2   = (exp(r1)-1)./(exp(r2)-exp(r1));

    for i  = 1:length(w1)
        u  =
sqrt((wd(i).*A1(i).*exp(r1(i).*y)+wd(i).*A2(i).*exp(r2(i).*y)+wd(i))./g);
        uprime = u-trapz(y,u);
        K(i) = -trapz(y,uprime.*cumtrapz(y,cumtrapz(y,uprime)));
    end
```

APPENDIX B STABILIZATION DATA

Table 7. Stabilization data

U/u_*	B/H	λ	ϕ_2	
16	6.448529	0.13	0.02	0.005
30.88889	6.448529	0.13	0.02	0.005
45.77778	6.448529	0.13	0.02	0.005
60.66667	6.448529	0.13	0.02	0.005
75.55556	6.448529	0.13	0.02	0.005
90.44444	6.448529	0.13	0.02	0.005
105.3333	6.448529	0.13	0.02	0.005
120.2222	6.448529	0.13	0.02	0.005
135.1111	6.448529	0.13	0.02	0.005
150	6.448529	0.13	0.02	0.005
41.83333	3	0.13	0.02	0.005
41.83333	4.666667	0.13	0.02	0.005
41.83333	6.333333	0.13	0.02	0.005
41.83333	8	0.13	0.02	0.005
41.83333	9.666667	0.13	0.02	0.005
41.83333	11.33333	0.13	0.02	0.005
41.83333	13	0.13	0.02	0.005
41.83333	14.66667	0.13	0.02	0.005
41.83333	16.33333	0.13	0.02	0.005
41.83333	18	0.13	0.02	0.005
41.83333	6.448529	0.13	0.02	0.005
41.83333	6.448529	0.152222	0.02	0.005
41.83333	6.448529	0.174444	0.02	0.005
41.83333	6.448529	0.196667	0.02	0.005
41.83333	6.448529	0.218889	0.02	0.005
41.83333	6.448529	0.241111	0.02	0.005
41.83333	6.448529	0.263333	0.02	0.005
41.83333	6.448529	0.285556	0.02	0.005
41.83333	6.448529	0.307778	0.02	0.005
41.83333	6.448529	0.33	0.02	0.005
41.83333	6.448529	0.13	0	0
41.83333	6.448529	0.13	0.003889	0.003889
41.83333	6.448529	0.13	0.007778	0.007778
41.83333	6.448529	0.13	0.011667	0.011667
41.83333	6.448529	0.13	0.015556	0.015556
41.83333	6.448529	0.13	0.019444	0.019444

41.83333	6.448529	0.13	0.023333	0.023333
41.83333	6.448529	0.13	0.027222	0.027222
41.83333	6.448529	0.13	0.031111	0.031111
41.83333	6.448529	0.13	0.035	0.035